


**Statistical analysis of chiral structured ensembles: Role of matrix constraints**

Triparna Mondal and Pragya Shukla

*Department of Physics, Indian Institute of Technology, Kharagpur, India* (Received 11 July 2018; revised manuscript received 22 November 2018; published 14 February 2019)

We analyze the statistical properties of complex systems with specific conservation laws and symmetry conditions which lead to various constraints and thereby structures in their matrix representation. An increase of constraints leads to a variation of the spectral statistics from Wigner-Dyson to Poisson limits, but the eigenfunction statistics remains weakly multifractal in the bulk. For some constraints, the statistics not only lies between the two limits but is size-independent too, thus indicating a critical point. Our results also reveal an important trend: While the spectral statistics is strongly sensitive to the number of independent matrix elements, the eigenfunction statistics seems to be affected mainly by their relative strengths. This is contrary to a previously held belief of a one-to-one relation between the statistics of the eigenfunctions and eigenvalues (e.g., associating Poisson statistics to the localized eigenfunctions and Wigner-Dyson statistics to delocalized ones). This also indicates the existence of new universality classes based on the matrix constraints (different from the 10 already-known symmetry-based classes).

DOI: [10.1103/PhysRevE.99.022124](https://doi.org/10.1103/PhysRevE.99.022124)**I. INTRODUCTION**

The missing information due to complexity in a system manifests itself by full or partial randomization of the matrix representations of the operators. The statistical behavior of the complex system can then be described by an appropriate random matrix ensemble based on the system-specific considerations. The conditions that influence nature of the ensemble can be divided into two types: (i) the “matrix” constraints (e.g., conservation laws and symmetries), which affect the broad structure of a single matrix through transformation properties and collective relations among the elements, and (ii) the “ensemble” constraints (e.g., disorder, dimensionality, and boundary conditions), which manifest themselves through the ensemble parameters, i.e., the distribution properties of matrix elements and/or the local relations among them [1]. In the past, there have been many studies of the ensembles with the matrix constraints related to unitary and antiunitary symmetries [2–5]. But information about the ensembles with matrix constraints based on conservation laws, which lead to specific relations among matrix elements, is still missing. The appearance of such cases in wide range of complex systems, e.g., disordered systems [6–8], complex and neural networks [9–13], and financial markets [14], make their statistical studies highly desirable. This motivates the present study in which we seek and analyze a specific class of “matrix” constraints which may affect the eigenfunction localization (spread of eigenfunctions in the basis-space) in a way similar to the influence of disorder (which is an ensemble constraint). Our primary focus in this work is to probe the influence of matrix constraints on the connection between degree of localization of eigenfunctions and the nature of spectral statistics.

The underlying symmetries of a system, e.g., continuous or discrete, unitary, anti-unitary, or their combinations, can manifest as matrix constraints if the basis for the matrix-representation of the operator, e.g., generator of the dynamics,

is chosen appropriately. For analysis of the physical properties, it is useful to choose the symmetry preserving basis which in turn puts the constraints on the type of matrix elements and/or structure of the matrix [3,15,16]. For example, the matrix turns out to be block-diagonal in the presence of the unitary symmetries but the chiral symmetry, an antiunitary one and referred to here as  $\mathcal{C}$ , leads to an off-diagonal block structure [3]. The particle-hole symmetry, again an antiunitary type and referred to here as  $\mathcal{P}$ , results in both diagonal and off-diagonal blocks. In the presence of another antiunitary symmetry such as time-reversal, referred to here as  $\mathcal{T}$ , the matrix is real-symmetric but is complex Hermitian. Based on the combination of these three fundamental antiunitary symmetries, the statistical behavior of complex systems can be classified into 10 universality classes of random matrix ensembles (based on their transformation properties) [3,16]. A violation of any of the symmetries can lead to a transition of statistics from one universality class to another [1]. In the past, the effect of symmetry as well as its violation on the statistical properties of the spectrum and eigenfunction dynamics has been studied extensively [2–4]. The presence of conservation laws along with symmetries, however, may lead to new structures in the matrix. Although a special class of structures have been studied in the recent past [17–19], the information about the role of generic structures in the eigenfunction localization is still missing. In the present work, we attempt to fulfill this gap by an analysis of some structured Hermitian matrix ensembles representing systems with two fundamental symmetry combinations, namely, chiral with time-reversal and chiral with no time-reversal [20].

Based on the nature of constraints, a matrix can display a range of structures, e.g., circulant, Toeplitz, column and row constraint, Henkel, in full form or in block form, with elements as real, complex, or quaternion [9,17,19,21,22]. Appearance of such structured matrices in many areas of physics was already known in the past, but their statistical

properties were not well-studied so far due to mathematical complexity involved in their analysis. The latter, however, can no longer be avoided due to recent applications of such matrices in the areas of huge technological potential, namely, artificial intelligence and complex networks. For example, a reduction of the computational complexity of large-scale neural networks leads to the structured matrices [9,12,13,23]. This is based on a size-manipulation of the weight matrix, an important basic tool describing the relation between input and output of a neural network for the deep neural network algorithms. (The latter are one of the most successful machine learning strategies, extensively applied, e.g., for speech recognition, computer vision, and classification of large data sets.) Based on the requisite training of the neural network, the weight matrix can be of various forms, unstructured as well as structured. An unstructured weight matrix can also be compressed to a structured form without losing much accuracy while achieving high compression ratio and high speedup for a broad category of network models (known as in deep non-negative matrix factorization (NMF) technique, a typical model for data representation and feature extraction) [23]. (Note, although the weight matrix, say  $W$ , is usually non-Hermitian, the stability analysis of the network is often based on the Hermitian matrix  $W^\dagger W$ ).

In general, many properties of complex systems can in principle be described in terms of the eigenfunctions and eigenvalues of the related matrices. This motivates the present study in which our main objective is to analyze the effect of matrix constraints on the relationship between eigenvalues and eigenfunctions. As mentioned above, the matrix constraints can be of many types resulting in a wide range of statistical behavior but this study is confined to a specific type, namely, chiral ensembles with real or complex entries which lead to a crossover of spectral statistics from Poisson to chiral Wigner-Dyson universality class. Note, for Hermitian matrices without any other constraint except symmetry, such a crossover is known to be associated with a localization-to-delocalization transition of eigenfunction dynamics (referred to as LD transition hereafter) [1,2,24]. The motivation to consider the ensembles with chirality and with or without time-reversal symmetry originates from multiple reasons. This not only helps us to analyze the role of two fundamental symmetries along with other matrix constraints, but the chirality also preserves the Hermitian nature of the matrices which is relevant for application to a wider range of real physical systems [8]. It must be indicated here that a consideration of Hermitian matrices rules out applicability of our results to a large class of complex networks represented by non-Hermitian matrices, e.g., biological and ecological networks, but the analytical approach presented here can be generalized, with some technical variations, to analyze the non-Hermitian cases as well as other symmetry cases.

The dimensionality of the system is another important matrix constraint which governs the sparsity of the matrix [1,24]. This along with the ensemble constraints (e.g., type of randomness of the matrix elements) plays a significant role in the eigenfunction localization. For a specific set of matrix constraints, it is well known that a LD transition of the eigenfunctions can be brought about by varying one of the local constraints, e.g., disorder; a well-known example

in this context is the Anderson transition [24,25]. Here we consider the reverse question: Can the above transition be brought about by varying matrix constraints for a fixed set of local constraints (while keeping the symmetries invariant to keep the transformation class of the ensemble unchanged)? In this context, it is important to indicate that a criterion for Anderson transition is the existence of a size-independent spectral statistics different from both metal and insulator regimes, thus implying a new universality class, at the critical point [24,25]. The standard Anderson ensemble, however, belongs to a class of Hermitian ensembles with symmetry as the only matrix constraint. The question is therefore whether a similar critical statistics can exist for the structured Hermitian ensembles with additional matrix constraints? As discussed later, we indeed find the evidence of critical spectral statistics for four of the five cases considered here. (Note, the term ‘‘critical statistics’’ is usually applied to nonequilibrium statistics, which remains distinct from equilibrium universality classes even in infinite-size limit.)

The paper is organized as follows. In Sec. II, we consider a chiral matrix subjected to five different types of matrix constraints and discuss their effect on the eigenvalues and eigenfunctions for each case. In the case of a complex system, some or all matrix elements are expected to be random and one needs to consider an ensemble of such matrices. To compare the effect of different constraints on the statistics, we choose an ensemble of matrices which consists of the identical and independent distribution (i.i.d.) of the free matrix elements, in each of the five cases. As described in Sec. III, this ensures an analogous form of the ensemble density for the five cases (required for the comparison of their statistical properties), which is then used to derive the joint probability distribution function (JPDF) of the eigenvalues and eigenfunctions. The latter, in principle, can be used to derive the JPDF of the eigenvalues only or the eigenfunctions only and their fluctuation measures, but the correlations among them, caused by the constraints, makes an exact derivation technically difficult and approximations are necessary. The insight into the statistical behavior can, however, be gained by an analysis of the terms present in the JPDF; this is discussed in Sec. IV. A numerical verification of our theoretical predictions is presented in Sec. V. We conclude in Sec. VI with a review of our main results and open questions.

## II. HERMITIAN MATRICES WITH CHIRALITY AND OTHER CONSTRAINTS

A generic  $(2N + \nu) \times (2N + \nu)$  chiral Hamiltonian  $H$  is given by

$$H = \begin{pmatrix} 0 & C \\ C^\dagger & 0 \end{pmatrix}, \quad (1)$$

where  $C$  is a general  $N \times (N + \nu)$  real, complex, or quaternion matrix (based on the nature of exact antiunitary symmetry of  $H$ ). The spectral and eigenfunction statistics of the matrix  $H$  depends on the nature of  $C$ . For  $C$  subjected to Hermitian constraint only, the spectral as well as eigenfunction correlations in the bulk of the spectrum can be modeled by the Wigner-Dyson universality classes [1,3–5,15,16]. In the presence of chirality, however, an additional level repulsion

appears around zero of the spectrum (the origin), which leads to different local spectral correlations near zero and away from the bulk [16,26,27].

For a simple exposition of the influence of constraints on the eigenvalues and eigenfunctions, we choose  $C$  as a real nonsymmetric  $N \times N$  matrix with  $\Lambda$  as its eigenvalue matrix and  $U^T, V$  as the left and right eigenvector matrices, respectively:  $U^T C V = \Lambda$  with  $U^T V = I$  and  $I$  as the identity matrix. The left and right eigenvectors  $U_n, V_n$  ( $n$ th columns of  $U, V$ , respectively) of  $C$ , corresponding to the eigenvalue  $\lambda_n$ , are then given by the following relation:

$$U_n^T C = \lambda_n U_n^T, \quad C V_n = V_n \lambda_n. \quad (2)$$

With  $H$  given by Eq. (1), let  $E$  be its eigenvalue matrix ( $E_{mn} = e_n \delta_{mn}$ ) and  $O$  as the eigenvector matrix, with  $O_{kn}$  as the  $k$ th component of the eigenvector  $O_n$  corresponding to eigenvalue  $e_n$ . Equation (2) along with Eq. (1) then implies that the eigenvalues of  $H$  exist in equal and opposite pairs; let us refer to such pairs as  $e_n, e_{n+N}$  with  $e_n = -e_{n+N}$ ,  $1 \leq n \leq N$ . The eigenvector pair  $O_n, O_{n+N}$  corresponding to eigenvalue pair  $e_n, e_{n+N}$  can, in general, be written as  $\begin{pmatrix} X_n \\ \pm Y_n \end{pmatrix}$  with  $X_n, Y_n$  as column vectors with  $N$  real components. Equation (1) then gives  $C Y_n = e_n X_n$  and  $C^\dagger X_n = e_n Y_n$ , which leads to  $C^\dagger C Y_n = e_n^2 Y_n$  and  $C C^\dagger X_n = e_n^2 X_n$ . The orthogonality condition  $O_n^\dagger O_{n+N} = 0$  along with normalization  $O_n^\dagger O_n = 1$  further gives [30]

$$X_n^\dagger X_n = Y_n^\dagger Y_n = 1/2. \quad (3)$$

With  $C$  as a  $N \times N$  square matrix, it has  $\beta N^2$  free parameters, with  $\beta = 1, 2, 4$  for  $C$  real, complex, or quaternion matrix, respectively. Introduction of new ‘‘matrix’’ constraints results in correlations among the matrix elements and reduces the number, say  $M$ , of the free parameters. Here we consider following five cases of the matrix  $C$ , given in a sequence of increasing level-repulsion (discussed later).

#### A. Case 1: Column-constraint circulant matrix

For  $C$  as a  $N \times N$  circulant matrix [28] with its elements  $C_{kl} = c_{(k-l) \bmod N}$ , with  $k, l = 1 \rightarrow N$ , we have the number of independent elements  $M = \beta N$ . Further imposing the column as well as row constraints, i.e.,

$$\sum_{k=1}^N C_{kl} = \sum_{k=1}^N C_{lk} = \alpha, \quad (4)$$

with  $\alpha$  as a constant, same for each column and row,  $M$  is further reduced:  $M = \beta(N - 1)$ . The circulant constraint on  $C$  leads to the same right and left eigenvector matrices, i.e.,  $U^T = V$  and both  $C, C^\dagger$  have same set of eigenvectors. This in turn implies  $U_n$  as the eigenvector of  $C C^\dagger = C^\dagger C$  with eigenvalue  $|\lambda_n|^2$ . Further, as  $\lambda_n = \lambda_{N-n}^*$  for  $n < N$ , the eigenvalue pairs of  $H$  matrix  $e_n, e_{n+N}$  appears with  $e_n = |\lambda_n|, e_{n+N} = -|\lambda_n|$ . This gives  $X_n = Y_n = \eta (U_n + (1 - \delta_{nN}) U_{N-n})$ , where the real constant  $\eta$  can be determined by the orthogonality condition on  $O_n$ .

As clear from the above,  $H$ , given by Eq. (1), has four matrix constraints (i) chiral symmetry, (ii) Hermiticity, (iii) circulant constraint, and (iv) column row constraint. Hereafter, this case will be referred to as the column-constraint chiral

matrix with circulant off-diagonal blocks. The spectral properties of this case was considered in detail in Ref. [29] and is included here for a comparison with other cases. As discussed in Ref. [29], all eigenvectors of  $H$  (i.e.,  $O_n, n = 1, \dots, 2N$ ) for this case remain extended.

#### B. Case 2: Toeplitz matrix

Next, we consider  $C$  as a  $N \times N$  Toeplitz matrix with elements defined as [28]

$$C_{kl} = C_{(k+r),(l+r)} = c_{(k-l)}, \\ \forall k, l = 1 \rightarrow N \text{ and } r = 1 \rightarrow N - k, N - l. \quad (5)$$

The absence of circulant as well as column constraint in  $C$  reduces the correlations among its matrix elements and increases the number of its independent parameters  $M = (2N - 1)\beta$ . The constraints on  $H$  are now (i) chirality, (ii) Hermiticity, and (iii)  $H_{k,N+l} = H_{k+r,N+l+r} = c_{(k-l)}$  for all  $k, l$  pairs and it becomes a  $2N \times 2N$  chiral matrix with Toeplitz off-diagonal blocks. This in turn leads to [30]

$$\sum_{n=1}^N e_n (X_{nk}^* X_{nl} - X_{n,k+r}^* X_{n,l+r} + Y_{nk}^* Y_{nl} - Y_{n,k+r}^* Y_{n,l+r}) = 0. \quad (6)$$

The above relations being valid for any  $(k, l)$  pair, this indicates strong correlations among almost all eigenfunctions of  $H$  (except for those with eigenvalue approximately zero) and only one of them, say  $O_1$ , is independent. Another relation following from the trace of  $C$  is  $\sum_{n=1}^N \lambda_n = \sum_{k=1}^N H_{k,N+k} = N H_{k,N+k}$ , which can be rewritten as [30]

$$\sum_{n=1}^N \lambda_n = N \sum_{n=1}^N e_n (X_{nk}^* X_{nk} + Y_{nk}^* Y_{nk}), \text{ for } k = 1, \dots, N. \quad (7)$$

The above relation although not used in present analysis is an important relation connecting the eigenvalues of  $C$  with the eigenfunctions of  $H$ .

#### C. Case 3: Column constraint matrix with same diagonals

$C$  is now obtained by relaxing the Toeplitz constraint and by imposing the column as well as row constraint along with the condition that all diagonal elements are equal. The diagonals  $C_{kk}$  can then be written as

$$C_{kk} = C_{11} = \alpha - \sum_{n=2}^N C_{1n} = \alpha - \sum_{n=2}^N C_{n1}, \\ \text{for } k = 1, \dots, N. \quad (8)$$

The off-diagonals of  $C$  are randomly chosen while keeping the sum of those in a column or row as constant. This increases the number of independent elements in  $C$  with  $M = \beta(N^2 - 3N + 3)$ .  $H$  is now subjected to four type of constraints (i) chirality, (ii) Hermiticity, (iii) column and row constraint, and (iv)  $H_{k,N+k} = H_{l,N+l}$  for all  $k = 1 \rightarrow N$  (using

$C_{kl} = H_{k(N+l)}$ . The latter in turn gives [30]

$$\sum_{n=1}^N e_n (X_{nk}^* X_{nk} - X_{nl}^* X_{nl} + Y_{nk}^* Y_{nk} - Y_{nl}^* Y_{nl}) = 0, \quad (9)$$

which again indicates the correlations among eigenfunction components (those with nonzero eigenvalues) but now the number of independent components is increased (as expected due to the increased number of independent matrix elements). Also as the relation  $\sum_{n=1}^N \lambda_n = \sum_{k=1}^N C_{kk} = N C_{kk}$  is still satisfied, this again leads to condition Eq. (7).

Further, as discussed in Ref. [31], the eigenvectors of a Hermitian matrix with column and row constraints but without chiral symmetry satisfy following conditions:  $\sum_{k=1}^{2N} O_{kn} = \pm\sqrt{2N} \delta_{nN}$  for  $n = 1 \rightarrow 2N$ . Generalization of these results to include chirality gives conditions on  $X_n$  and  $Y_n$  for  $1 \leq n \leq N$  [30]:

$$\sum_{k=1}^N (X_{kn} + Y_{kn}) = \pm\sqrt{2N} \delta_{nN} \text{ for } e_n, \quad (10)$$

$$\sum_{k=1}^N (X_{kn} - Y_{kn}) = \pm\sqrt{2N} \delta_{nN} \text{ for } e_{n+N}. \quad (11)$$

This in turn implies  $X_{kN} = Y_{kN} = \pm\frac{1}{\sqrt{2N}}$  or  $X_{kN} = -Y_{kN} = \pm\frac{1}{\sqrt{2N}}$  for  $k = 1 \rightarrow N$ .

#### D. Case 4: Upper Toeplitz matrix

Another form of  $C$  can be obtained by removing the diagonal constraints from  $C$  but imposing a variant of the Toeplitz constraint. The latter corresponds to the Toeplitz condition only among the elements of the diagonal and the upper diagonal of  $C$  but with no constraint imposed on the lower diagonals:

$$C_{k,l} = C_{(k+r),(l+r)} = c_{(k-l)}, \quad \text{for } k \leq l \text{ and } r=1 \rightarrow N-l. \quad (12)$$

Consequently, the number of independent elements in  $C$  now become  $M = \beta N(N+1)/2$  (note, here  $C$  is *not* a symmetric matrix). The matrix  $H$  is now subjected to three types of constraints: (i) chirality, (ii) Hermiticity, and (iii)  $H_{k,N+l} = c_{(k-l)}$  for  $k \leq l$ . Clearly Eq. (7) is again valid for this case, but Eq. (6) is now applicable only for  $k \leq l$ . Note the number of independent eigenfunction components here is higher than cases 1 and 2 but is less than case 3.

#### E. Case 5: Column-constraint matrix

With  $C$  subjected only to the constraint Eq. (4), it now has  $\beta(N^2 - 2N + 1)$  free parameters. This in turn implies three types of constraints on  $H$ : (i) chiral symmetry, (ii) Hermiticity, and (iii) column and row constraints. The eigenvectors of  $H$  are now subjected to conditions Eqs. (10) and (11) besides orthogonality and normalization. As the number of constraints in this case are minimum, this results in an increased number of independent eigenfunction components.

### III. ENSEMBLES WITH CHIRALITY AND OTHER CONSTRAINTS

For matrices representing complex systems, it is imperative to consider their ensembles, which can subsequently be used to derive the JPDF of their eigenvalues and eigenfunctions and other related properties. Consider the ensemble density  $\rho(H)$  of  $H$ . Using the transformation from matrix space to eigenvalue-eigenvector space, the JPDF  $P(E, O) \equiv P(e_1, \dots, e_N; O_1, \dots, O_N)$  can be expressed as

$$P(E; O) = J(E, O|H) \rho(H), \quad (13)$$

with  $J(E, O|H)$  as the Jacobian of transformation from  $H$ -matrix space to  $E, O$  space. As expected,  $J$  depends on the matrix constraints, which in turn are sensitive to the choice of basis and are expected to manifest primarily through basis-dependent properties of the matrix, i.e., eigenfunction components. The eigenvalues, being basis-independent, are subjected to the constraints when the basis preserves a specific symmetry. For Hamiltonian with chiral symmetry besides other constraints, therefore, the basis, which preserves the chirality, imposes the constraint  $e_n = -e_{N+n}$ . But other constraints manifest through the eigenvector components. Thus, for a  $2N \times 2N$  chiral Hermitian matrix with  $M$  independent elements (their total number as  $\beta N^2$ ),  $N$  eigenvalues and  $M - N$  eigenvector components can be chosen as independent without any loss of generality. This leads to  $J$  as a  $M \times M$  determinant consisting of first order derivatives of independent  $H$  elements with respect to  $N$  independent eigenvalues and  $M - N$  independent parameters. Following the same steps as given in Ref. [4], it can be written as  $J(E, O|H) = \Delta_N(e) f(O)$ , where  $f(O)$  and  $\Delta_N(e)$  depend on the matrix constraints:  $\Delta_N(e) = 1$  for cases with  $M = N$  but for cases with  $M > N$ , one has

$$\Delta_N(e) \equiv \Delta_N(e_1, e_2, \dots, e_N) = \prod_{k \leq l=1}^N |e_k^2 - e_l^2|^\beta, \quad (14)$$

with  $\beta = 1$  if  $H$  is a real-symmetric matrix,  $\beta = 2$  for  $H$  complex Hermitian. It is important to note here that, for cases  $M > N$ ,  $\Delta_N(e)$  is of the same form as that of a chiral matrix with Hermitian constraints only.

To proceed further, we need to determine  $\rho(H)$ . Following from Eq. (1),

$$\rho(H) = \rho_c(C) F_c F_h, \quad (15)$$

with  $\rho_c(C)$  as the probability density of the ensemble of  $C$  matrices, with  $F_h(H) = \delta(H - H^\dagger)$  and  $F_c = \prod_{k,l=1}^N \delta(H_{kl})$  as the constraints due to Hermiticity and chirality of  $H$ , respectively. For cases where  $\rho_c(C)$  is not known, one can invoke the maximum entropy hypothesis: The system is best described by the distribution  $\rho_c(C)$  that maximizes Shannon's information entropy  $I[\rho_c(C)] = -\int \rho_c(C) \ln \rho_c(C) d\mu(C)$  under known set of ensemble constraints, e.g., on the moments of the entries of  $C$ . It must be emphasized that a specific set of matrix constraints can lead to many different ensembles.

For simple exposition of our ideas, here we consider the set of ensemble constraints which leads to a Gaussian distribution for all independent parameters  $c_\mu$  of  $C$ , with  $\mu = 1, \dots, M$

each with same variance and zero mean:

$$\rho_c(C) = \mathcal{N} \exp \left[ -\gamma \sum_{\mu=1}^M c_\mu^2 \right] F_n, \quad (16)$$

with  $\mathcal{N}$  as a normalization constant,  $M$  as the total number of independent parameters in  $C$ , and  $F_n$  as the function implementing the matrix constraints on  $C$ . An important point to note here is that a rescaling of  $c_\mu$  by  $\sqrt{\gamma}$  renders  $\rho(C)$  and thereby  $\rho(H)$  free of any parameters. Further the Gaussian form of  $\rho_c$  in Eq. (16) is a consequence of the ensemble constraints on the first- and second-order moments of  $c_\mu$ . The ensemble constraints on higher-order moments of  $c_\mu$  in general lead to a non-Gaussian ensemble of chiral constraint matrices. (Note, a most generic form of  $\rho_c$  can be given in terms of an arbitrary distribution, say  $\rho_0$  of the free matrix elements  $c_j$ , with  $j = 0 \rightarrow M$ :  $\rho_c(C) = \mathcal{N} \rho_0(c_1, c_2, \dots, c_M) F_n$ , with  $F_n$  dependent on the matrix constraints.)

Equation (16) along with Eq. (15) gives  $\rho(H)$ , which can be used to derive  $P(E; O)$ . As discussed below, the steps depend on the type of matrix constraints.

#### A. Case 1

With only  $\beta(N-1)$  free parameters, Eqs. (15) and (16) and the relation  $C_{kl} = H_{k,N+l}$  gives

$$\rho(H) = \mathcal{N} \exp \left[ -\frac{\gamma}{N} \sum_{k,l=1}^N |H_{k(N+l)}|^2 \right] F_1 F_c F_h, \quad (17)$$

where the function  $F_1$  describes the circulant as well as the column and row constraint on  $C$ :

$$F_1 \equiv \delta \left[ \sum_{l=1}^N H_{1(N+l)} - \alpha \right] \prod_{k,l=1}^N \delta[H_{k(N+l)} - c_{(k-l) \bmod N}]. \quad (18)$$

As the eigenvectors for all circulant matrices are same and with constant components [29],  $C$  and therefore  $H$  varies with respect to its eigenvalues only which leads to  $J_H(e, O|H) = \text{constant}$ . The eigenvalue distribution in this case can be given as [29]

$$P_e(e_1, \dots, e_{2N}) = \mathcal{N} \exp \left[ -\frac{\gamma}{N} \sum_{m=1}^N e_m^2 \right] \times \prod_{n=1}^N \delta(e_n + e_{n+N}) \delta(e_N - \alpha). \quad (19)$$

Note, here  $\Delta_N(e) = 1$ . As clear from the above, the lack of repulsion among eigenvalues permits their clustering although all eigenvectors (i.e.,  $O_n, n = 1, \dots, 2N$ ) remain extended.

#### B. Case 2

With the number of independent parameters now increased to  $(2N-1)\beta$ , Eqs. (15) and (16) along with Eq. (5) lead to

$$\rho(H) = \mathcal{N} \exp \left[ -\gamma \sum_{k,l=1}^N \alpha_{kl} |H_{k(N+l)}|^2 \right] F_2 F_c F_h, \quad (20)$$

with

$$\alpha_{kl} = \frac{1}{N - |k-l|}, \quad (21)$$

and  $F_2$  now refers to Toeplitz constraint on  $C$ :  $F_2(H) \equiv \prod_{k,l=1}^N \delta[H_{k(N+l)} - c_{(k-l)}]$ .

Substitution of the relation  $H_{kl} = \sum_{n=1}^{2N} e_n O_{nk}^* O_{nl}$  and  $e_n = -e_{N+n}$  in Eq. (20) and using Eqs. (13) and (14),  $P(E, O)$  can now be written as

$$P(E, O) = \mathcal{N} \Delta_N \exp \left[ -\gamma \sum_{m,n=1}^N e_m e_n \sum_{k,l} \alpha_{kl} S_{mnkl} \right] \mathcal{F}_2, \quad (22)$$

with

$$S_{mnkl} = (X_{nk}^* X_{nl} + Y_{nk}^* Y_{nl})(X_{mk} X_{ml}^* + Y_{mk} Y_{ml}^*) \quad (23)$$

and

$$\begin{aligned} \mathcal{F}_2(E, X, Y) \\ \equiv f(O) \mathcal{F}_{\text{ch}} \prod_{k,l=1}^N \delta[X_k^\dagger E_+ X_l - Y_k^\dagger E_+ Y_l - c_{(k-l)}]. \end{aligned} \quad (24)$$

Here  $f(O)$  in the above equation arises from the Jacobian contribution, the  $\delta$  function implies condition Eq. (6) and  $E_+$  refers to the  $N \times N$  diagonal matrix with  $E_{+,mn} = e_n \delta_{mn}$  with  $n = 1 \rightarrow N$ .  $\mathcal{F}_{\text{ch}}$  is the function describing the combined effect of Hermitian and chirality constraints on the eigenvectors and eigenvalues:

$$\mathcal{F}_{\text{ch}}(E, X, Y) \equiv \prod_{n=1}^N \delta(e_n + e_{n+N}) \delta \left( X^\dagger X - \frac{1}{2} \right) \delta \left( Y^\dagger Y - \frac{1}{2} \right). \quad (25)$$

Equation (3) implies

$$\sum_{m=1}^N \sum_{k,l=1}^N \alpha_{kl} S_{mnkl} = \sum_{n=1}^N \sum_{k,l=1}^N \alpha_{kl} S_{mnkl} = \frac{4}{2N}. \quad (26)$$

This on substitution in Eq. (22) leads to [30]

$$P(E, O) = \mathcal{N} \Delta_N(e) \exp \left[ -\frac{\gamma}{2N} \sum_{n=1}^N e_n^2 - \frac{\gamma}{2} \sum_{n,m=1}^N (e_n - e_m)^2 T_{mn} \right] \mathcal{F}_e, \quad (27)$$

where  $\mathcal{F}_e \equiv \mathcal{F}_2$  and  $T_{mn} = \sum_{k,l=1}^N (1 - \alpha_{kl}) S_{mnkl}$ . The latter can be rewritten as

$$T_{mn} = \left( 1 - \frac{1}{N} \right) \mathcal{C}(m, n) + \sum_{k,l=1; k < l}^N (1 - \alpha_{kl}) (S_{mnkl} + S_{mnkl}^*), \quad (28)$$

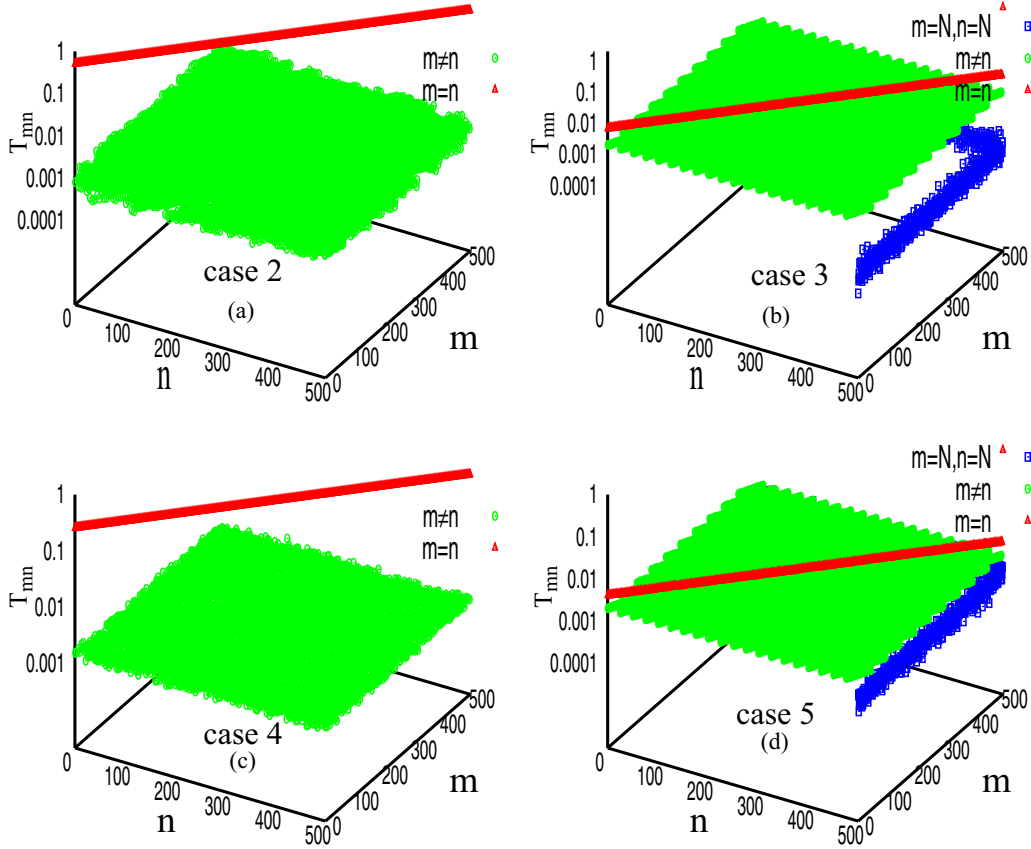


FIG. 1. Eigenfunction correlations: The figure displays  $T_{mn}$  [Eq. (28)] dependence for many  $m, n$  values for a single matrix of size  $2N = 1000$  in each case (without ensemble averaging). Clearly, for each case,  $T_{mn} \propto 1/N$ , except for  $T_{mm}$  which is larger than  $1/N$ . Note, for cases 3 and 5 (which correspond to column constraint matrices with  $\alpha = 0$ ),  $T_{mN}$  and  $T_{Nn}$  also differ from  $1/N$ .

where  $\mathcal{C}(m, n)$  is the correlation between the eigenfunctions  $O_n$  and  $O_m$ :

$$\begin{aligned} \mathcal{C}(m, n) &= \sum_{k=1}^{2N} |O_{kn}|^2 |O_{km}|^2 \\ &= \sum_{k=1}^N (|X_{nk}|^2 + |Y_{nk}|^2)(|X_{mk}|^2 + |Y_{mk}|^2). \end{aligned} \quad (29)$$

As clear from the above,  $\mathcal{C}(m, n) > 0$ . Further note, for  $P(E, O)$  to be finite,  $T_{mn}$  must be semipositive. The numerics discussed in Sec. V indeed indicates  $T_{mn} \sim 1/N$  for all  $(m, n)$  pairs with  $m \neq n$  (see Fig. 1), which follows from Eq. (28) if one assumes an extended dynamics of almost all eigenfunctions, implying same order of magnitude for their components (although their signs can vary); this behavior is also indicated by the analysis of fractal dimension  $D_q$  [25] depicted in Fig. 4.

### C. Case 3

Under the constraint Eq. (8) and using Eqs. (15) and (16),  $\rho(H)$  can be written as

$$\rho(H) = \mathcal{N} \exp \left[ -\gamma H_{1,N+1}^2 - \gamma \sum_{k,l=1; k \neq l}^{N-1} H_{k,N+1}^2 \right] F_3 F_c F_h \quad (30)$$

$$= \mathcal{N} \exp \left[ -\frac{\gamma}{N} \sum_{k=1}^{N-1} H_{k,N+k}^2 - \gamma \sum_{k,l=1; k \neq l}^{N-1} H_{k,N+l}^2 \right] F_3 F_c F_h, \quad (31)$$

with  $F_3 \equiv \prod_{l=1}^N \delta(H_{l,N+l} - H_{1,N+1}) \delta[\sum_{k=1}^N H_{k,N+l} - \alpha]$ .

Proceeding as in the previous case,  $P(E, O)$  can again be rewritten as in Eq. (27), with  $T_{mn}$  again given by Eq. (28), but now

$$\alpha_{kk} = \frac{1}{N}, \quad \alpha_{kl} = 1, \quad \alpha_{kN} = \alpha_{Nl} = 0, \quad \forall k, l < N, \quad (32)$$

and  $\mathcal{F}_e \equiv \mathcal{F}_3$ , where

$$\begin{aligned} \mathcal{F}_3(E, O) &\equiv f(O) \mathcal{F}_{ch} \prod_{k=1}^N \delta(X_k^\dagger E_+ X_k - Y_k^\dagger E_+ Y_k) \\ &\quad \times \delta[A^T (X_k + Y_k) - \sqrt{2N} b_k], \end{aligned} \quad (33)$$

with  $A$  as a column vector of size  $N$  with entries  $A_m = 1$  for  $m = 1 \rightarrow N$ ,  $b_N = 1$ ,  $b_k = 0$  for  $k \neq N$  and  $E_+$  defined below Eq. (24). Note the condition Eqs. (9)–(11) are taken into account by the  $\delta$  functions in Eq. (33).

To gain insight in the spectral statistics, we again need to analyze  $T_{mn}$ . Equation (23) along with Eqs. (10) and (11) lead to identities  $\sum_{k=1}^N S_{mnkN} = \delta_{mn}$  and  $S_{mnNN} = \frac{1}{4N^2}$ . These help

to rewrite  $T_{mn}$  as

$$T_{mn} = \left(1 - \frac{1}{N}\right) C_{mn} + 2 \sum_{k=1}^{N-1} S_{mnkN} \approx C_{mn} + 2 \left( \delta_{mn} - \frac{1}{4N^2} \right). \quad (34)$$

Note as  $C_{mn} > \frac{1}{N^2}$ , here again  $T_{mn} > 0$ , which is again confirmed by our numerics discussed in Sec. V (see Fig. 1).

#### D. Case 4

Under the constraint Eq. (12) along with Eqs. (15) and (16),  $\rho(H)$  now becomes

$$\rho(H) = \mathcal{N} \exp \left[ -\gamma \sum_{k,l=1;k>l}^N H_{k,N+l}^2 + \sum_{k,l=1;k \leq l}^N \frac{\gamma}{N - |k-l|} H_{k,N+l}^2 \right] F_4 F_c F_h, \quad (35)$$

with  $F_4 \equiv \prod_{k,l=1;k>l}^N \delta[H_{k,N+l} - c_{(k-l)}]$ .

Following the same steps as in case 2,  $P(E, O)$  can be rewritten as Eq. (27) but with the following changes:  $T_{mn}$  is again given by Eq. (28) but with

$$\alpha_{kl} = 1 \quad \text{for } k > l, \quad \alpha_{kl} = \frac{1}{N - |k-l|} \quad \text{for } k \leq l, \quad (36)$$

and

$$\mathcal{F}_4(E, O) \equiv f(O) \mathcal{F}_{\text{ch}} \prod_{k \leq l=1}^N \delta[X_k^\dagger E_+ X_l - Y_k^\dagger E_+ Y_l - c_{(k-l)}], \quad (37)$$

with  $E_+$  as defined below Eq. (24). Here again  $T_{mn}$  can be rewritten as

$$T_{mn} \approx C(m, n) + \sum_{k=1}^N \sum_{r=1}^{N-k} \left(1 - \frac{1}{N-r}\right) S_{mnkk+r}. \quad (38)$$

Here again the numerics indicates  $T_{mn} \sim O(1/N)$  (see Fig. 1).

#### E. Case 5

In the presence of only column constraints and chirality,  $\rho(H)$  can be written as

$$\rho(H) = \mathcal{N} \exp \left[ -\gamma \sum_{k,l}^{N-1} |H_{k(N+l)}|^2 \right] F_5 F_c F_h, \quad (39)$$

with  $F_5 \equiv \prod_{l=1}^N \delta(\sum_{k=1}^N H_{k,N+l} - \alpha)$ .

Here again  $P(E, O)$  can be written as in Eq. (27) with  $T_{mn}$  again given by Eq. (28) but with

$$\alpha_{kl} = 1 - \delta_{kl} \quad \forall k, l = 1 \rightarrow N. \quad (40)$$

(Alternatively, one can choose  $\alpha_{kl} = 1$ ,  $\alpha_{kN} = \alpha_{Nl} = \alpha_{NN} = 0$  for  $k, l = 1 \rightarrow (N-1)$ ; as expected, this does not affect

the statistics.) The constraint on the eigenvalues and eigenfunctions now becomes

$$\mathcal{F}_5(E, O) \equiv f(O) \mathcal{F}_{\text{ch}} \prod_{k=1}^N \delta[A^T(X_k + Y_k) - \sqrt{2N}b_k]. \quad (41)$$

Here the term with  $\delta$ -function implies the condition Eqs. (10) and (11). Note  $T_{mn}$  in this case can be rewritten as

$$T_{mn} = \mathcal{C}(m, n) > 0, \quad (42)$$

where  $C_{mn}$  is given by Eq. (29). Here again numerics indicates  $T_{mn} \sim \frac{1}{N}$  (see Fig. 1).

As discussed in detail in Ref. [31], the distribution  $P(E, O)$  for a Hermitian matrix with column constraint but without chirality has the same form as in the present case except for an additional constraint described by Eq. (25).

## IV. SPECTRAL STATISTICS

As mentioned in Sec. III,  $\rho(H)$  is a parameter-free, maximum entropy distribution. Consequently the eigenvalues and eigenfunctions of  $H$  tend to distribute in a way to maximize the JPDF  $P(E, O)$  under the given set of constraints. As discussed in the previous section,  $P(E, O)$  for the cases 2–5 is given by Eq. (27) but  $T_{mn}$  and  $\mathcal{F}_e$  in each case are different; here  $T_{mn}$  is given by Eqs. (28), (34), (38), and (42) and  $\mathcal{F}_e = \mathcal{F}_2, \mathcal{F}_3, \mathcal{F}_4, \mathcal{F}_5$ , respectively. In principle, the information about various spectral and/or eigenfunction measures can now be obtained by integrating Eq. (27) over irrelevant variables but the presence of constraints  $\mathcal{F}_e$  make it technically difficult.

Equation (27), however, reveals an important underlying connection:  $P(E, O)$  in Eq. (27) is equivalent to that of a Brownian ensemble with chirality (with  $\mathcal{F}_e = f(O) \mathcal{F}_{\text{ch}}$  for the latter case). The latter corresponds to an ensemble of Hermitian matrices  $H$  given by Eq. (1) with the matrix elements of  $C$  distributed as independent Gaussian variables [of mean  $\langle C_{kl} \rangle = 0$  and variance  $\langle |C_{kl}|^2 \rangle - \langle C_{kl} \rangle^2 = \delta_{kl} + \kappa (1 - \delta_{kl})$ ], with  $\kappa$  being an arbitrary constant; here the matrix  $H$  is not subjected to any other constraint except chiral and time-reversal symmetries (no time reversal if  $\beta = 2$ ). In the regions where contribution of  $\mathcal{F}_e$  is negligible, the spectral statistics of cases 2–5 is therefore expected to resemble that of a chiral Brownian ensemble which in turn is connected to a wide range of other unstructured ensembles (see, for example, Ref. [32] for a related discussion).

Further insights about expected spectral behavior can be gained as follows. Besides  $\mathcal{F}_e$ ,  $P(E, O)$  in Eq. (27) consists of three other terms, namely,  $\Delta_N(e)$  and two sums in the exponent. The first term in the exponent acts as a confining potential on the mutually repelling eigenvalues; with  $P(E, O)$  rapidly decaying for  $e_n \gg \sqrt{2N}$ , this indicates the support of the spectrum to be of the order of  $\sqrt{2N}$ . The statistics at short energy ranges is governed by  $\mathcal{F}_e$  as well as the competition between two terms containing the eigenvalue repulsion i.e.,  $\Delta_N$  and  $\mathcal{S} \equiv \frac{1}{N} \sum_{n=1}^N e_n^2 + \sum_{n,m=1}^N (e_n - e_m)^2 T_{mn}$ . For a clearer understanding, the individual role of each term can be described as follows:

$\mathcal{F}_e$ : The constraints in each case contain a sum over second order short as well as long-range eigenfunction correlations which can restrict the dynamics of eigenvalues in a way to

enhance  $P(E, O)$ . This however affects the eigenvalues in the regions  $e \neq 0$  only,

$\Delta_N$ : analogous to classical chiral ensembles e.g. chiral GOE and chiral GUE [3], the presence of  $\Delta_N$  in Eq. (14) tends to support the JPDF  $P(E; O)$  with repulsion among eigenvalues. The tendency in the present case is however affected by the presence of other terms i.e those in the exponent and the constraints.

$\mathcal{S}$ : as clear from Eq. (27), a smaller exponent therein gives rise to a larger  $P(E; O)$ . This in turn requires

$$\mathcal{S} \equiv \frac{1}{N} \sum_{n=1}^N e_n^2 + \sum_{n,m=1}^N (e_n - e_m)^2 T_{mn} < 1. \quad (43)$$

Here, for cases 2–5,  $T_{mn} > 0$ . Further, intuition based on previous studied suggests that  $T_{mn} \sim o(1/N)$  for the cases in which all independent matrix elements are identically distributed; this conjecture is confirmed by our numerical analysis for cases 2–5, discussed in the next section and displayed in Fig. 1. Thus, based on Eq. (43), a reduction of the term  $\sum_n e_n^2$  as well as the separations of type  $(e_n - e_m)^2$  results in a larger  $P(E; O)$ ; (note, due to presence in the exponent,  $\mathcal{S}$  dominates over  $\Delta_N$ ). The above in turn implies a reduced density of states  $\langle \rho(e) \rangle$  near the spectrum edge  $|e| \sim \sqrt{N}$  and its increase in the bulk (for energies  $|e| < \sqrt{N}$ ).

Clearly, the contribution from the three terms, mentioned above, depends on the location of eigenvalues as well as their density along the spectrum. As the fluctuations of local mean level density  $\langle \rho_e(e) \rangle$  at an arbitrary energy  $e$  are measured in units of the local mean level spacing  $D(e) = \frac{1}{\langle \rho(e) \rangle}$ , this in turn renders the local-statistics nonstationary (varying along the spectrum axis). For local fluctuation analysis, therefore, it is appropriate to consider the eigenvalues in units of the local mean level spacing (also known as the unfolded spectrum). Equation (43) can then be rewritten as a sum over local conditions on the rescaled eigenvalues  $r_n = \frac{e_n}{D(e)}$ , with one such condition in the neighborhood of an arbitrary energy  $e$  implying

$$\frac{1}{N} \sum_{n \in (e)} r_n^2 + \sum_{m, n \in (e)} (r_n - r_m)^2 T_{mn} < \langle \rho(e) \rangle^2. \quad (44)$$

Here the notation  $\sum_{m, n \in (e)}$  implies a local summation, i.e., over contributions from the spectral range around  $e$ , i.e., over  $e_m, e_n \sim e$  only.

The behavior of local fluctuations in two main regions can now be described as follows:

$e \sim 0$ : As  $\mathcal{F}_e$  does not influence the behavior near  $e \sim 0$ , the statistics in this region is dominated by the condition Eq. (44). The latter, however, is sensitive to  $\langle \rho(e) \rangle$  which itself depends on the matrix constraints (see Figs. 5 and 6). As a consequence, the statistics in this region can change with the constraints. Clearly, for the cases with  $\langle \rho(e) \rangle \rightarrow 0$ , i.e., relatively large mean level spacing, Eq. (44) supports level clustering in the local fluctuation measures. The statistics is therefore expected to approach Poisson limit. For the cases where  $\langle \rho(e) \rangle$  is large, the condition is satisfied even for  $r_n - r_m \sim o(1)$ , i.e., if the eigenvalues  $e_n, e_m$  lie at the distances of the order of mean level spacing; this results in the fluctuations indicating a level-repulsion at  $e$  with statistics closer to

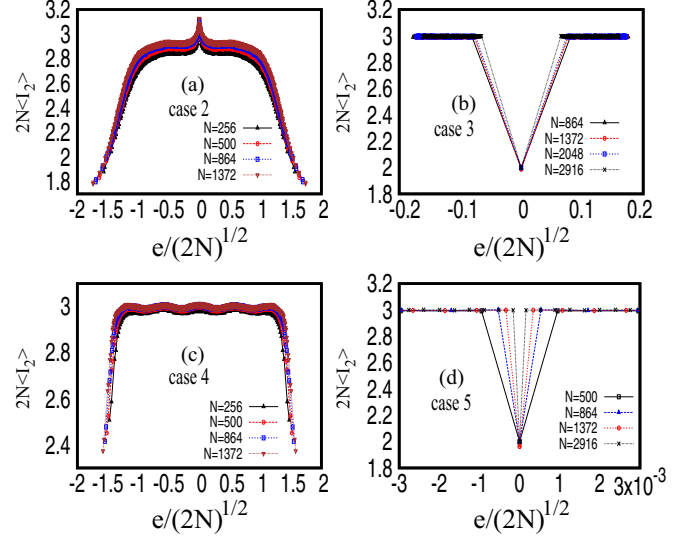


FIG. 2. Signatures of extended eigenfunctions: The figure describes the energy-dependence of the ensemble-averaged inverse participation ratio  $\langle I_2 \rangle$  for many system sizes; the number of matrices in each ensemble is chosen to ensure the same finite-size error. As clear,  $\langle I_2 \rangle \propto \frac{1}{N}$  for almost all energies for each case, implying eigenfunctions extended in whole basis. But  $\langle I_2 \rangle \gg 1/N$  for the eigenfunctions corresponding to the largest eigenvalues in cases 3 and 5, which indicates their localization [note that panels (b) and (d) are displayed without the largest pairs of eigenvalues; see Fig. 3 for them]. Also note that, for the cases with column-constraint (i.e., cases 3 and 5),  $\langle I_2 \rangle = 1/N$  at  $e = 0$  (which is expected for the eigenfunction corresponding to eigenvalue  $e_n = \alpha = 0$ ). A size-analogy for each case also follows on the rescaling  $e \rightarrow e/\sqrt{2N}$ ,  $\langle I_2 \rangle \rightarrow \langle I_2 \rangle \times (2N)$ .

Wigner-Dyson type. Similarly for the case, in which  $\langle \rho(e) \rangle$  satisfies  $\sum_{m,n}^e (r_n - r_m)^2 \approx \langle \rho(e) \rangle^2$  near  $e \sim 0$ , the statistics in the range is expected to be intermediate to Poisson and Wigner-Dyson limits.

$e \neq 0$ : the above behavior is now moderated by the eigenvalue-eigenfunctions correlations present in  $\mathcal{F}_e$ ; the eigenvalues for the case with higher number of eigenfunction correlations are intuitively expected to be less independent to move faraway even if the local spectral density is large. Note, the mean level density for regions  $e \neq 0$  is almost same for all the cases, implying same contribution from  $\mathcal{S}$ . The statistics, however, is expected to change from Poisson to GOE, as the number of constraints decrease. To confirm this behavior we pursue a detailed numerical analysis described in next section.

An important point worth indicating here is as follows: with  $T_{mn} \propto 1/N$ , a rescaling  $e \rightarrow e\sqrt{N}$  reduces the JPDF in Eq. (27) in a size-independent form. The spectral as well as the eigenfunctions statistics is therefore expected to be size-independent; this is indeed verified by our numerical analysis discussed in next section (see Figs. 2 and 4 for the size-independence of the eigenfunction measures and Figs. 8–11 for the spectral statistics). But as discussed above, based on the matrix constraints and concerned energy-range, the spectral statistics may approach Poisson or chiral Wigner-Dyson limits, or may lie intermediate to these limits; in the latter case, it is referred as critical. Further, for the energy



ranges where  $\mathcal{F}_e$  can be ignored (e.g.,  $e \sim 0$ ), the statistics is expected to be analogous to that of a critical Brownian ensemble with chiral symmetry.

## V. NUMERICAL ANALYSIS

The theoretical formulation given in Sec. III clearly reveals the analogies and differences of the five ensembles. For example, the JPDF in each case can be written in terms of Eq. (27) with only  $\mathcal{F}_e$  part varying from one case to the other. Further, as discussed in Sec. IV, the analysis in Sec. III not only provides clear insights about the energy-dependence of the fluctuations for a given case but also indicates the existence of a critical point of statistics. To reconfirm our theoretical predictions, we pursue a numerical statistical analysis of these cases and generate the ensembles of  $H$  matrices for cases 1–5 as follows. The independent matrix elements in each case are chosen as independent Gaussian variables (with zero mean and unit variance); the rest of the elements are then obtained by invoking the respective matrix constraints. The eigenvalues and eigenfunctions of  $H$  for each of the five ensembles are computed by standard LAPACK subroutines for exact diagonalization of the Hermitian matrices.

The theoretical analysis in previous section is based on the conjecture  $T_{mn} \sim 1/N$  (with  $T_{mn}$  given by eq. (28); as illustrated in Fig. 1, this is indeed confirmed for each case. This in turn suggests the following behavior of a typical eigenfunction component, say  $O_{kn}$ , in each case;  $|O_{kn}| \propto \frac{1}{\sqrt{N}}$ . To verify the latter, we analyze the inverse participation ratio (IPR)  $I_2$ , a standard tool to describe the localization behavior [25]. For an eigenfunction  $O_n$  corresponding to an eigenvalue  $e_n$ , it is defined as  $I_2(O_n) = \sum_{k=1}^N |O_{kn}|^4$ . Following from the definition,  $I_2(O_n) \propto 1/N$  for an eigenfunction extended throughout a basis-space of size  $N$ , and  $I_2(O_n) = 1$  for an eigenfunction localized on just one basis state. In general, IPR varies with energy and it is a standard practice to consider an averaged  $I_2$  of all eigenfunctions within a given spectral range in which the average spectral density varies smoothly. But, as discussed below and displayed in Figs. 5 and 6, the latter shows a rapid variation for some specific energy ranges, i.e.,  $e = 0$  as well as near spectrum-edges and it is more appropriate to consider the ensemble averaged  $I_2$ , referred as  $\langle I_2 \rangle$  at a specific energy instead of the spectral averaged one.

The IPR-analysis of the eigenfunctions for case 1 was discussed in Ref. [29], which indicated that  $I_2(O_n) = \frac{3}{4N}$  for  $n \neq N, 2N$  and  $I_2(O_N) = I_2(O_{2N}) = \frac{1}{2N}$ . For the case  $\alpha = 0$ , however,  $\lambda_N = 0$ , which results in a degenerate eigenvalue pair  $e_N, e_{2N} = 0$  with corresponding eigenvectors as  $\begin{pmatrix} U_N \\ 0 \end{pmatrix}$  and  $\begin{pmatrix} 0 \\ U_N \end{pmatrix}$ . As a consequence,  $I_2(O_N) = I_2(O_{2N}) = \frac{1}{N}$  for the case  $\alpha = 0$ .

In the present work, we numerically analyze cases 2–5. As displayed in Fig. 2,  $\langle I_2(e) \rangle \approx \frac{3}{2N}$  for almost all  $e$ -ranges for these cases. Further, for the cases with column-constraints (i.e., cases 3 and 5),  $\langle I_2 \rangle$  for the eigenfunction  $O_N$  is  $\approx 1/N$  (see Figs. 2(b) and 2(d), respectively); note, for column constant  $\alpha = 0$ ,  $O_N$  corresponds to the eigenvalue  $e_N = 0$ . This indicates an extended dynamics, in the basis-space, for almost all eigenfunctions of each of the five cases, irrespective of the number of constraints. Clearly if the ensemble averaged

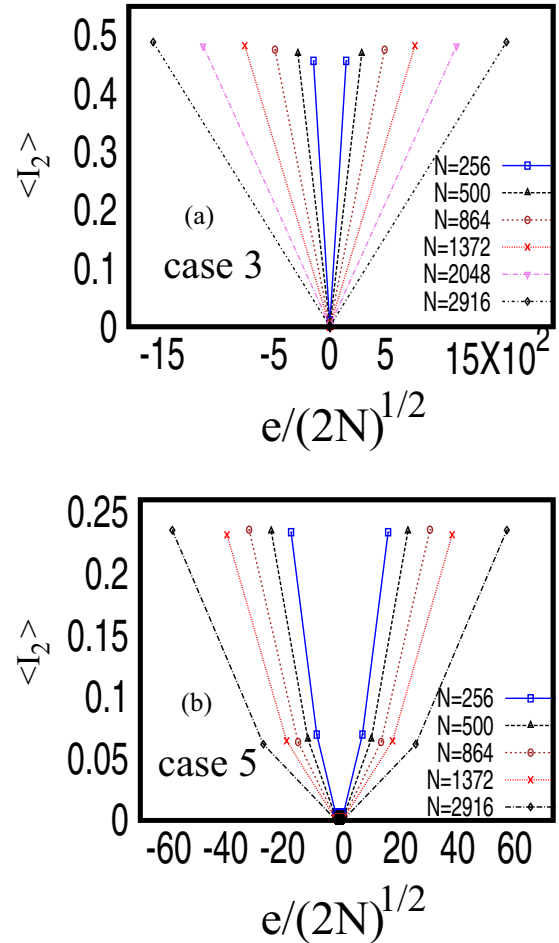


FIG. 3. Localization of eigenfunctions: This figure displays  $\langle I_2 \rangle$  for the eigenfunctions corresponding to largest eigenvalues for cases 3 and 5. For case 3,  $\langle I_2 \rangle = 1/2$  corresponding to largest eigenvalue pair (a), but for case 5, there are two pairs of extreme eigenvalues with  $\langle I_2 \rangle = 1/4$  and  $\approx 1/20$  (b). A higher value of  $\langle I_2 \rangle (\gg 1/N)$  indicates a localization of corresponding eigenfunction to fewer basis sites.

inverse participation ratio is used as the criteria, the eigenfunction statistics for these cases is not sensitive to the matrix constraints; note the disorder-strength  $\gamma$  is same for all the independent elements in each case (see Sec. III). A variation of disorder-strength among independent matrix elements is however expected to affect the eigenfunction dynamics; such a response is indeed confirmed for the column constraint ensembles without chirality [31,33].

Another point worth indicating here is the following. For the cases 3 and 5, the largest eigenvalue pairs are isolated lying quite far away from the bulk and the  $\langle I_2 \rangle$  for corresponding eigenfunctions are much larger than  $\frac{1}{2N}$  which indicates their localization. As shown in Fig. 3(a) for case 3,  $\langle I_2(O_1) \rangle = \langle I_2(O_{N+1}) \rangle = 1/2$  for the eigenfunctions corresponding to largest eigenvalue pair  $e_1, e_{N+1}$ . This is indeed consistent with condition Eq. (43), implying a localization of the corresponding eigenfunctions if  $|e_n - e_m| \approx \sqrt{2N}$ . Note in case 5 there are two such pairs of localized eigenfunctions with  $\langle I_2 \rangle = 1/4$  and  $1/20$  [Fig. 3(b)].

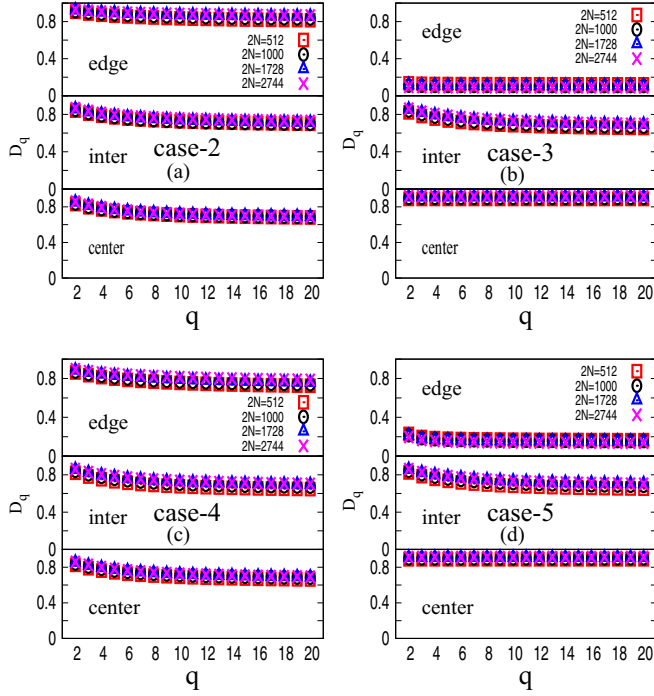


FIG. 4. Fractal dimension  $D_q$ : The figure describes the size as well as energy-dependence of the ensemble-averaged fractal dimension  $D_q$  for the cases 2–5. Here, edge inter(mediate) and center regions correspond to energies  $e \sim e_0 \times \sqrt{2N}$  with  $e_0 \sim -2, -0.75, 0$ , respectively. With  $D_q \approx 0.7$  in the intermediate energy range of each case, the figure indicates the multifractality of the eigenfunctions in the regime. The behavior indicating localization ( $D_q \ll 1$ ) and delocalization ( $D_q \sim 1$ ) for case 3 in the edge and center region, respectively, is similar to that of case 5; note both cases are subjected to column constraints. But an almost delocalized ( $D_q \sim 0.9$ ) and multifractal behavior ( $D_q \sim 0.6$ ) for case 2 (Toeplitz) in the edge and center region, respectively, is similar to another case without column constraint, i.e., case 4 (partial Toeplitz).

To rule out the possibility that higher order moments of the eigenfunctions may indicate localization, we also analyze  $\langle I_q \rangle$  for  $q > 2$ . Its size-dependence is a frequently used characteristic of the eigenfunctions's multifractality [25],  $\langle I_q \rangle \propto (2N)^{-(q-1)D_q}$ , where  $D_q$  is the fractal dimension. For localized eigenfunction,  $D_q = 0$ , whereas it increases to system dimension  $d$  as localization decreases, with  $0 < D_q < d$  an indicator of the multifractality. Note each ensemble considered in our study corresponds to  $d = 1$ . Figure 4 displays the  $q$ -dependence of the  $D_{qN} = -\frac{1}{q-1} \frac{\langle \ln I_q \rangle}{\ln(2N)}$  for many system sizes; note  $D_q = \lim_{N \rightarrow \infty} D_{qN}$ . As clear from the insets,  $D_{qN}$  for large  $q$  is less than 1 near  $e \sim 0$  and  $e \sim -0.75\sqrt{2N}$  for some of the cases which indicates weak multifractality of the eigenfunctions in those energy ranges. Our numerical analysis of  $D_{qN}$ , for many  $N$  values of each case, indicates its size-independence.

An analysis of the spectral fluctuations requires a prior knowledge of the average spectral density which can be obtained by averaging over an ensemble, over a spectral range or both. The correct averaging procedure however depends on the ergodic nature of the spectrum [34]. This can be explained as follows. For complex systems, the density of

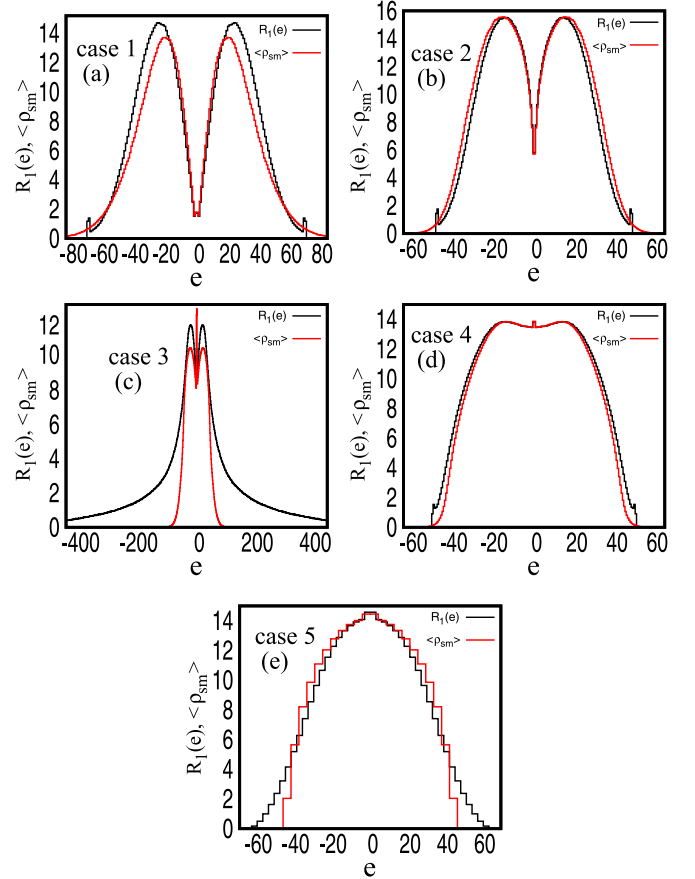


FIG. 5. Ergodicity in level density: Comparison between ensemble averaged level density  $R_1(e) \equiv \langle \rho_e \rangle$  and  $\langle \rho_{sm}(e) \rangle$  for matrix  $H$  of fixed size  $2N = 1000$  and an ensemble of 5000 matrices. An almost analogous behavior of  $R_1(e)$  and  $\langle \rho_{sm}(e) \rangle$  is visible for energy  $e \sim 0$  for all the cases with small nonnegligible deviation away from  $e \sim 0$  for cases 1, 2, 4, and 5, implying nearly ergodic level density for them. For case 3, however, panel (c) indicates a clear nonergodicity for the energy range other than  $e \sim 0$ .

states  $\rho_e$  at an energy  $e$ , defined as  $\rho_e(e) = \sum_{k=1}^N \delta(e - e_k)$ , can often be expressed as a superposition of the fluctuations over an average smooth background:  $\rho_e(e) = \rho_{sm}(e) + \rho_{fluc}$ . Here  $\rho_{sm}$  refers to the spectral average at  $e$ , defined as  $\rho_{sm} = \frac{1}{\Delta e} \int_{e-\Delta e/2}^{e+\Delta e/2} de \rho_e(e)$ , over a scale larger than that of fluctuations; i.e.,  $\int_{e-\Delta e/2}^{e+\Delta e/2} de \rho_{fluc}(e) = 0$ . For comparison of the fluctuations at an energy  $e$  (referred as local), therefore, it is necessary to first rescale each spectrum so as to have a same mean level density; this requires a prior information about  $\rho_{sm}(e)$ . In the case of an ergodic spectrum,  $\rho_{sm}(e)$  can, however, be replaced by  $R_1(e)$ , the ensemble averaged level density defined as  $R_1(e) = \langle \rho_e \rangle \equiv N \int P_e(e, e_2, \dots, e_N) \prod_{k=2}^N de_k$  [4]. Note here the ergodicity condition of  $\rho_e$  implies  $\langle \rho_{fluc} \rangle \rightarrow 0$  which leads to  $\langle \rho_{sm}(e) \rangle \approx \langle \rho_e(e) \rangle = R_1(e)$ , where  $\langle \cdot \rangle$  is an ensemble average for a fixed  $e$  [34] (see also Sec. 4.10 of Ref. [3]).

Figure 5 compares the  $R_1(e)$  as well as  $\langle \rho_{sm}(e) \rangle$  for an ensemble of matrices of fixed size ( $2N = 1000$ ) for each of the five cases. Here in case 3, a large deviation between the two curves indicates the nonergodic tendency of  $\rho_e$  whereas for

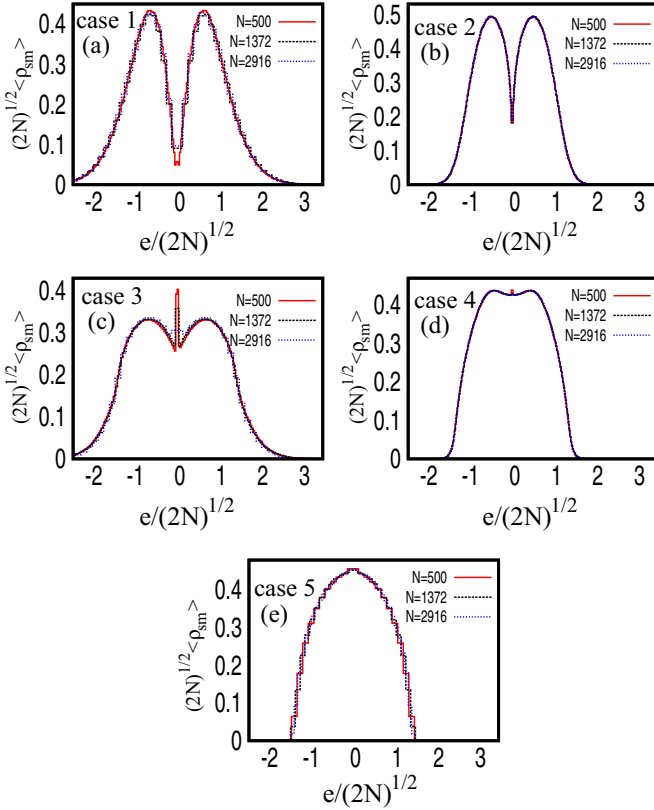


FIG. 6. Size-dependence of level density: This figure depicts the size-dependence of the  $\langle \rho_{sm} \rangle$  for the five cases. A rescaling of the energy  $e \rightarrow e/\sqrt{2N}$  along with  $\langle \rho_{sm} \rangle \rightarrow \langle \rho_{sm} \rangle \times \sqrt{2N}$  results in convergence of curves for different sizes in each case. Also note that  $\langle \rho_{sm} \rangle$  varies significantly from cases 1 to 5, which clearly reflects the effect of constraints on the mean level density.

other cases deviation is small, although not negligible, away from the region  $e = 0$ . The figure also reveals a drastic change of level-density from one case to the other, clearly indicating its strong sensitivity to the number of constraints. Interestingly, however, as displayed in Fig. 6, the rescaled  $\langle \rho_{sm}(e) \rangle$  remains size-independent for all the five cases (with rescaling  $e \rightarrow e/\sqrt{2N}$ ,  $\langle \rho_{sm} \rangle \rightarrow \langle \rho_{sm} \rangle \times \sqrt{2N}$ ), thus implying a same  $N$ -dependence for all of them.

Due to lack of ergodicity, we unfold the spectrum in each case by the local unfolding process; as described in detail in Ref. [35], the later is based on first obtaining a smoothed histogram of  $\rho_{sm}$  for each spectrum (i.e., for each matrix) followed by a numerical averaging (with unfolded levels given by  $r_n = \int_{-\infty}^{e_n} \rho_{sm} de$ ). Here we consider the local fluctuations for both high and low density regions of the spectrum and choose an optimized range  $\Delta e$  (5% of the total eigenvalues), sufficiently large for the good statistics with minimum mixing of different statistics; the chosen ranges are  $e \sim (-2 \pm 0.05) \times \sqrt{2N}$ ,  $\sim (-0.75 \pm 0.05) \times \sqrt{2N}$ ,  $\sim (0 \pm 0.03) \times \sqrt{2N}$ , later referred to as edge, bulk, and center, respectively). It is worth noting here that although the density in the bulk region is locally stationary, there is a rapid variation of  $\rho_{sm}$  in the edge as well as center for the cases with reduced number of independent parameters. Hence, for comparison in the edge and center, it is necessary to

choose levels within smaller spectral ranges. The statistics can however be improved by applying ensemble average along with spectral average.

For fluctuations-analysis, we consider two spectral measures namely the nearest-neighbor spacing distribution  $P(s)$  and the number-variance  $\Sigma^2(r)$ , the standard tools for the short and long-range spectral correlations, respectively [3,5]. Here  $P(s)$  is defined as the probability of two nearest neighbor eigenvalues to occur at a distance  $s$ , measured in units of local mean level spacing  $D$ , and  $\Sigma^2(r)$  as the variance in the number of levels in an interval of length  $r$  mean level spacings. As indicated by previous studies (see, for example, Refs. [1,3,4]), the level fluctuations of a system subjected only to Hermitian constraint along with time-reversal symmetry in a fully delocalized wave limit behave similar to that of a Gaussian orthogonal ensemble (GOE) [1,3,4] with  $P(s) = \frac{\pi}{2} s e^{-\frac{\pi}{4}s^2}$  and  $\Sigma^2(r) \approx \frac{2}{\pi^2} (\ln(2\pi r) + \gamma + 1 - \frac{\pi^2}{8})$  with  $\gamma = 0.5772$ . Similarly, the fully localized case shows a behavior typical of a set of uncorrelated random levels, that is, exponential decay for  $P(s)$ , also referred as Poisson distribution,  $P(s) = e^{-s}$ , and  $\Sigma^2(r) = r$ . But, as discussed in Ref. [29] for the case of chiral circulant matrices, Poisson spectral statistics appears along with delocalized eigenfunctions. This indicates the influence of constraints on the relation between statistics of the eigenvalues and eigenfunction which is further confirmed by the present study of other four cases.

Figure 7 compares  $P(s)$  and  $\Sigma^2(r)$  of the spectra for all five cases at three different energy ranges, namely, at bulk ( $e \sim -0.75 \pm 0.05) \times \sqrt{2N}$ , near center ( $e \sim 0 \pm 0.03) \times \sqrt{2N}$  and near edge ( $e \sim -2.0 \pm 0.05) \times \sqrt{2N}$ ; the ensemble in each case consists of 850 matrices of size  $2N = 5832$ . In the bulk, the level statistics changes from Poisson to GOE as the number of independent matrix parameters increase; as displayed in the figure, both  $P(s)$  and  $\Sigma^2(r)$  curves are very close to corresponding GOE statistics for the cases 3, 4, and 5, coincide with Poisson limit for the case 1 and are intermediate to Poisson and GOE (relatively nearer to Poisson) for the case 2. The change is slower near the center, with case 2 now moving closer to Poisson (compared to bulk) and case 3 now lying intermediate to Poisson and GOE. Near the edge, cases 4 and 5 also deviate from the GOE and move towards Poisson. Note the numerical behavior in all three regions is consistent with our theoretical prediction discussed in previous section.

It is important to note here that if one applies the same criteria as that for Hermitian ensembles with no other constraint except symmetry, the  $D_q$  behavior for these cases is often not consistent with that expected based on their spectral statistics. This can further be clarified as follows: Based on previous studies, a variation of spectral statistics from Poisson to GOE limit is usually accompanied by the eigenfunctions becoming increasingly delocalized, with  $D_q$  varying from  $0 \rightarrow 1$ , respectively. (Note, in the past, this has led to the use of Poisson and Wigner-Dyson spectral statistics as the criteria for the localized and delocalized eigenfunctions dynamics in the basis space [2]). This correspondence however is not applicable here. For example, for case 2, the spectral statistics in the bulk and center of spectrum is although not Poisson but relatively closer to Poisson limit [Figs. 8(a) and 8(b)], the eigenfunction behavior is therefore expected to be almost

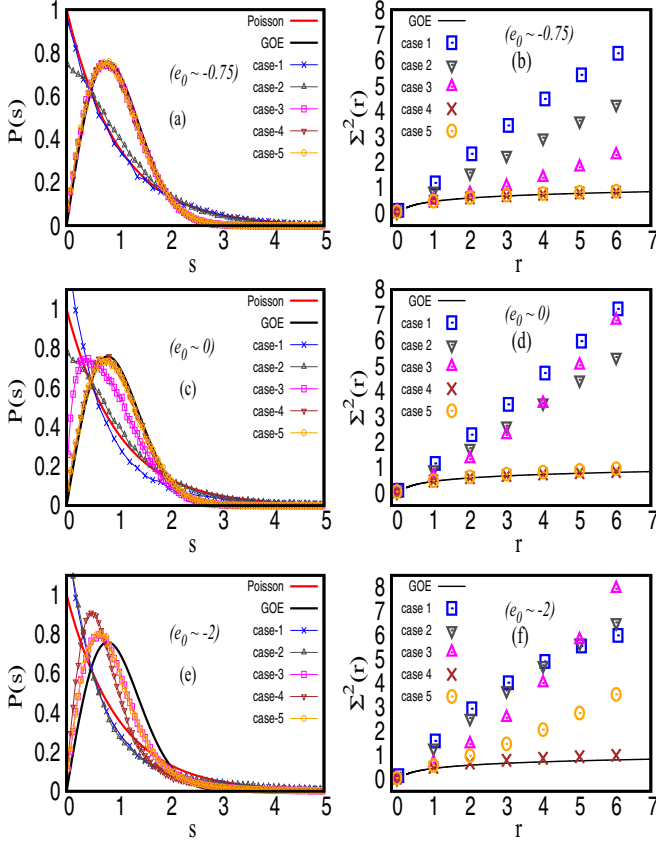


FIG. 7. Constraint dependence of spectral statistics:  $P(s)$  and  $\Sigma^2(r)$  for an ensemble of 850 matrices of size  $2N = 5832$  for cases 1–5 at three different spectral regimes (near  $e \sim e_0 \times \sqrt{2N}$ ): (a, b) at bulk ( $e_0 \sim -0.75$ ), (c, d) at center ( $e_0 \sim 0$ ), (e, f) at edge ( $e_0 \sim -2$ ). The behavior of both measures for cases 2, 3, 4, and 5 clearly indicates an energy dependence, with  $P(s)$  at a given energy changing from Poisson to GOE as the number of constraints decrease (thus, the free matrix elements increase). This behavior is also supported by  $\Sigma_2(r)$  statistics shown in panels (b, d, f).

localized implying  $D_q \ll 1$  but the numerics gives  $D_q \approx 0.7 - 0.8$  (Fig. 4), thus suggesting extended states with weak multifractality. Similarly, for case 3, the spectral statistics in the edge region is closer to GOE (Fig. 9), thus suggesting eigenfunctions to be almost delocalized with expected  $D_q \rightarrow 1$  but numerics gives  $D_q \sim 0.1$  (Fig. 4). Further, the statistics for case 3 near  $e \sim -0.75 \times \sqrt{2N}$  approaches GOE but is intermediate near  $e \sim 0$  (Fig. 9), which suggests  $D_q$  for the former to be larger than the latter; Fig. 4, however, shows a reverse trend.

Another important aspect revealed by our analysis is the existence of a critical statistics, located between Poisson and GOE limit, even when all free matrix elements are of the same order (see Ref. [32] for more details). Note in case of Hermitian matrix ensembles with no other constraint except symmetry, this occurs when the matrix is sparse (for example, see Refs. [24,32]). Here, the deviation of  $P(s)$  statistics from both Poisson and GOE limits in the center  $e \sim 0$  for cases 2 and 3, and, in the edge  $e \sim -2 \times \sqrt{2N}$  for cases 4 and 5 suggests the existence of a critical statistics. This motivates us

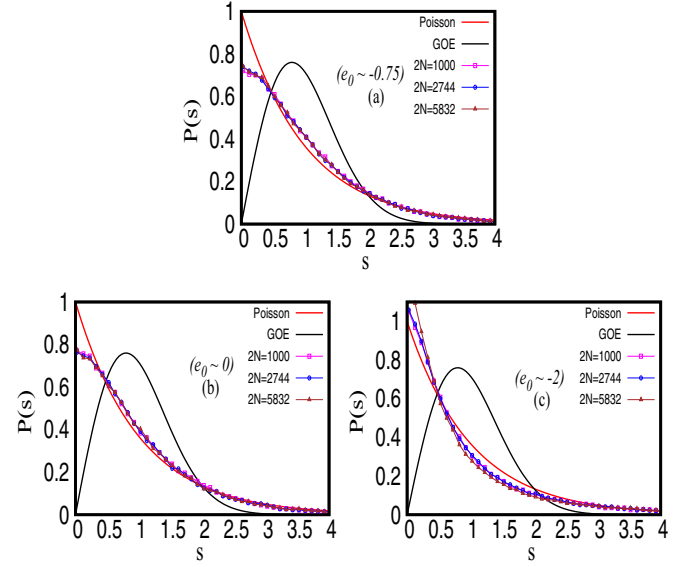


FIG. 8. Criticality for case 2: Here, a size-independence of the  $P(s)$  behavior in each energy range ( $e \sim e_0 \times \sqrt{2N}$  with  $e_0$  given in each figure) is clearly visible from the panels (a, b, c). Further,  $P(s)$ , at center as well as in the bulk, lies intermediate to both Poisson and GOE limits (although closer to Poisson but distinct from it), which implies a critical spectral statistics. At edge, the spectral statistics approaches Poisson for all system sizes (c).

to analyze the spectral statistics for many  $N$  values; here the ensemble size for each  $N$  is chosen so as to keep same total number of levels for the analysis. As displayed in Figs. 8–11, the short range statistics, i.e.,  $P(s)$  for the above cases is indeed size-independent, thus implying an intermediate state between Poisson and GOE even in an infinite size limit. This

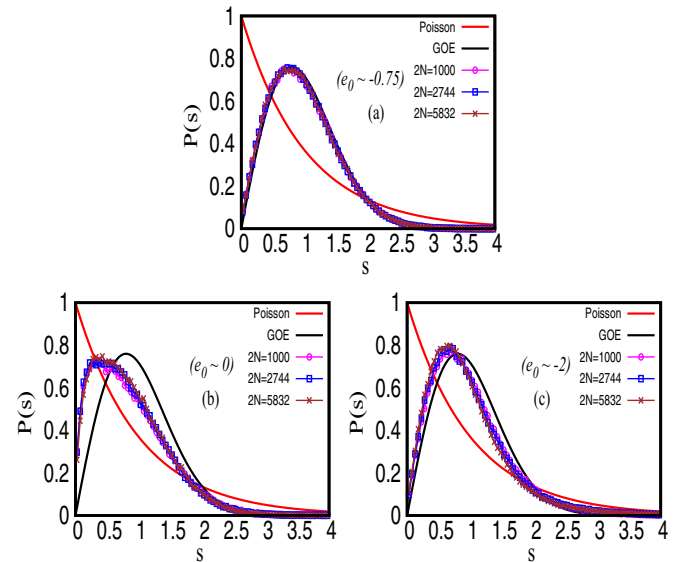


FIG. 9. Criticality for case 3: At bulk ( $e \sim e_0 \times \sqrt{2N}$  with  $e_0$  given in each figure), the spectral statistics approaches GOE for all system sizes (a). But at center as well as in the edge, a critical behavior of  $P(s)$ , size-independent as well intermediate to both Poisson and GOE limits, is clearly visible from panels (b) and (c).

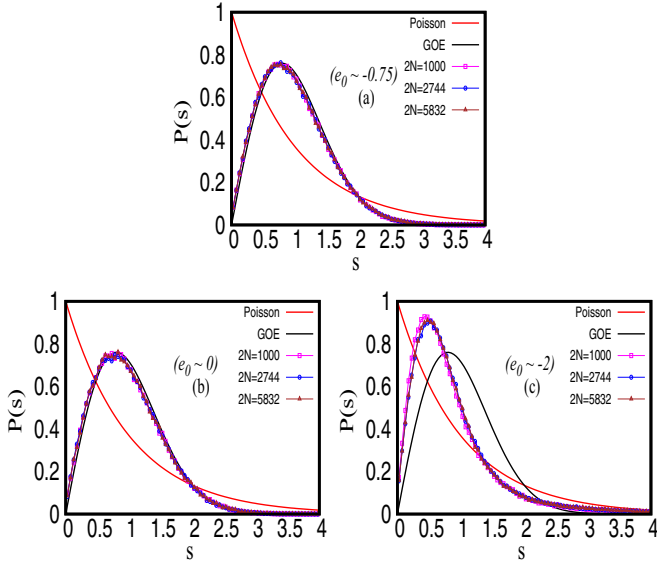


FIG. 10. Criticality for case 4: At bulk and center of the spectrum, the spectral statistics approaches GOE for all system sizes (a, b). But in the edge region, a critical behavior of  $P(s)$ , size-independent as well intermediate to both Poisson and GOE limits, is clearly visible from the part (c).

behavior is typical of a critical point of the spectral statistics [32]. This is also confirmed by a similar analysis for the size-dependence of  $\Sigma^2(r)$  for each case (figures not included in this work).

In the case of disordered Hamiltonians, a mobility edge is defined as the critical energy which separates the localized states from extended ones; in terms of the spectral statistics, this translates to Poisson and Wigner-Dyson statistics above

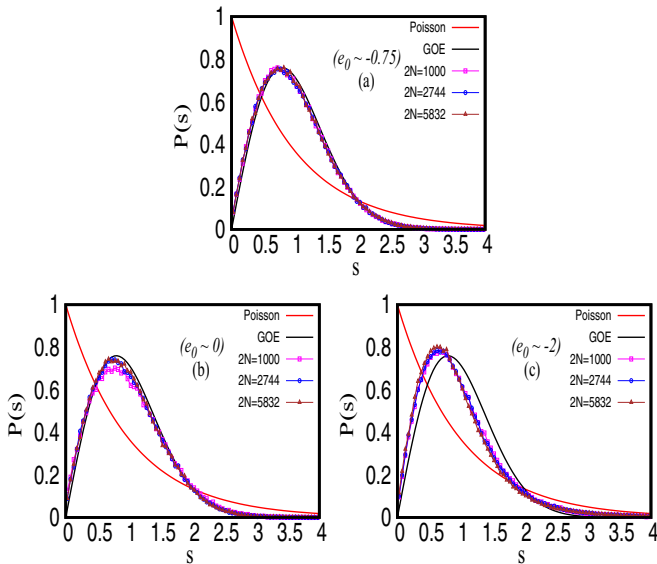


FIG. 11. Criticality for case 5: Similar to case 4, here again the spectral statistics in the bulk and center of the spectrum approaches GOE for all system sizes (a, b). But part (c) indicates a critical behavior of  $P(s)$ , size-independent as well intermediate to both Poisson and GOE limits.

and below the critical energy. But the Hamiltonians considered previously are usually those with no other constraint except those leading to Hermitian matrices. It is then relevant to question whether such a mobility edge can exist also for the Hamiltonians subjected to higher number of constraints? Note the spectral statistics for case 3 varies significantly with energy, from almost GOE type behavior (in the bulk) to an intermediate state between Poisson and GOE (in the center and edge). Although the IPR study for this case (shown in Fig. 2) indicates the extended states for almost all energies but  $D_q$  behavior is clearly energy-dependent (Fig. 4). This suggests the existence of a mobility edge in this case too.

### VI. CONCLUSION

Based on the present study of a few structured matrix ensembles, we find that the relation between the statistics of the eigenvalues and eigenfunctions of a generic random matrix ensemble is a lot more complicated than previously believed on the basis of Hermitian ensembles with symmetry as the only constraint. In fact it seems while the spectral statistics is primarily governed by the number of independent matrix parameters, the eigenvector statistics is sensitive to their relative degree of randomness. More clearly, as far as the independent matrix elements are statistically of the same strength (e.g., same mean and variance) irrespective of their number, it will always lead to almost all extended eigenfunctions (except for a very few strongly localized ones). The eigenvalue statistics however undergoes a significant change as the number of independent parameters vary. Our analysis also reveals the possibility of a critical statistics without changing disorder and just by imposing specific constraints. More clearly, it is possible to undergo a localization-delocalization transition without varying disorder or energy and just by imposing a specific set of constraints on the disordered Hamiltonians.

Another important aspect of our results is following: in analogy with standard Gaussian ensembles (i.e., Gaussian ensembles subjected only to Hermitian and chiral constraints, referred below as minimum-constraint case), each ensemble considered in this study is essentially parameter-free. But contrary to former, the latter are not only basis dependent but the statistics of eigenvalues and eigenfunctions for them is energy-dependent as well as different from the minimum-constraint cases and therefore represent new universality classes. Again, in analogy with previously known ten universality classes of Gaussian ensembles, these new universality classes also arise from different types of matrix constraints; but, while former are based on symmetry conditions, the latter belong to more complicated system conditions, e.g., a combination of conservation laws and symmetry conditions. Although the present work focuses only on five types of matrix constraints, it is possible to consider many other types, while keeping the ensemble free of parameters, which may lead to many new universality classes lying between Poisson and standard Gaussian cases. It is worth emphasizing that the matrix constraints considered here are not just pure academic pursuit, they arise in real physical situations too. For example, as discussed in Ref. [31], the ensembles with column constraints appear in a wide range of areas and the ensemble with topological constraints appear in disordered

systems [10]. Furthermore, a large range of matrix constraints can appear in a weight matrix, an important component of deep learning in artificial intelligence, and which depends on training of the neural network to a series of commands.

The present analysis suggests many new directions for future studies. Here we have considered ensembles subjected to many constraints but with their free elements independent and identically distributed; as confirmed by our numerics, the latter lead to weakly multifractal eigenstates in the bulk. It is relevant to know whether nonidentical distributions may lead to the eigenfunctions with strong multifractality and how will that affect the corresponding eigenvalue distributions. Further the existence of a critical statistics between Poisson

and Wigner-Dyson for a specific set of matrix constraints, with fractal dimension  $0 < D_q < 1$ , (as in cases 2 and 3) indicates the possibility of a localization-delocalization transition even for a very weak disorder and arbitrary dimensions if those constraints can be engineered in a disordered lattice (or more generally in a complex system). This also gives rise to the curiosity about the possibility of such a transition for other symmetry classes, e.g., particle-hole symmetries. Further, for applicability to a wider range of complex systems, e.g., complex networks with asymmetric couplings, a generalization of our analysis to non-Hermitian ensembles is also desirable.

- 
- [1] P. Shukla, *Int. J. Mod. Phys. B (WSPC)* **26**, 1230008 (2012).
- [2] T. Guhr, G. A. Muller-Groeling, and H. A. Weidenmuller, *Phys. Rep.* **299**, 189 (1998).
- [3] F. Haake, *Quantum Signatures of Chaos* (Springer, Berlin, 1991).
- [4] M. L. Mehta, *Random Matrices* (Academic Press, San Diego, 1991).
- [5] T. A. Brody, J. Flores, J. B. French, P. A. Mello, A. Pandey, and S. S. M. Wong, *Rev. Mod. Phys.* **53**, 385 (1981).
- [6] M. Mezard, G. Parisi, and A. Zee, *Nucl. Phys. B* **559**, 689 (1999); J. Staring, B. Mehlig, Y. V. Fyodorov, and J. M. Luck, *Phys. Rev. E* **67**, 047101 (2003); T. S. Grigera, V. Martin-Mayor, G. Parisi, and P. Verrocchio, *Phys. Rev. Lett.* **87**, 085502 (2001); *J. Phys.: Condens. Matter* **14**, 2167 (2002); *Nature* **422**, 289 (2003); M. Rusek, J. Mostowski, and A. Orlowski, *Phys. Rev. A* **61**, 022704 (2000); F. A. Pinheiro, M. Rusek, A. Orlowski, and B. A. van Tiggelen, *Phys. Rev. E* **69**, 026605 (2004); M. Antezza, Y. Castin, and D. A. W. Hutchinson, *Phys. Rev. A* **82**, 043602 (2010); S. E. Skipetrov and R. Maynard, *Phys. Rev. Lett.* **85**, 736 (2000); B. Spivak and A. Zyuzin, *ibid.* **84**, 1970 (2000); B. Gremaud and T. Wellens, *ibid.* **104**, 133901 (2010).
- [7] P. Shukla and I. Batra, *Phys. Rev. B* **71**, 235107 (2005).
- [8] V. Gurarie and J. T. Chalker, *Phys. Rev. B* **68**, 134207 (2003).
- [9] R. Qiu and M. Wicks, *Cognitive Networked Sensing and Big Data*, 1st ed. (Springer, New York, 2013).
- [10] H. Dai, Z. Geary, and L. P. Kadanoff, *J. Stat. Mech.* (2009) P05012.
- [11] B. Georgeot, O. Giraud, and D. L. Shepelyansky, *Phys. Rev. E* **81**, 056109 (2010).
- [12] Y. Ahmadian, F. Fumarola, and K. D. Miller, *Phys. Rev. E* **91**, 012820 (2015).
- [13] A. Amir, N. Hatano, and D. R. Nelson, *Phys. Rev. E* **93**, 042310 (2016).
- [14] D. Challet, M. Marsilli, and R. Zecchina, *Phys. Rev. Lett.* **84**, 1824 (2000).
- [15] F. Dyson, *J. Math. Phys.* **3**, 1191 (1962).
- [16] A. Altland and M. R. Zirnbauer, *Phys. Rev. B* **55**, 1142 (1997).
- [17] J. Grela and T. Guhr, *Phys. Rev. E* **94**, 042130 (2016).
- [18] P. Bourgade and H. T. Yau, *Commun. Math. Phys.* **350**, 231 (2017).
- [19] K. Truong and A. Ossipov, *J. Phys. A* **51**, 065001 (2018).
- [20] It is worth emphasizing here that the presence of any two of the three anti-unitary symmetries implies that the third is also present. Whenever a system has both  $\mathcal{T}$  and  $\mathcal{P}$ , there is also a chiral symmetry  $\mathcal{C} = \mathcal{P}\mathcal{T}$ . But, if both  $\mathcal{T}$  and  $\mathcal{P}$  are absent, then  $\mathcal{C}$  may or may not be present. However, if the system has either  $\mathcal{T}$  or  $\mathcal{P}$ , then it cannot have chiral symmetry.
- [21] D. Achlioptas, Random matrices in data analysis, in *Knowledge Discovery in Databases: PKDD 2004* (Springer-Verlag, Berlin/Heridelberg, 2004). P.1.
- [22] R. Couillet and M. Debbah, *Random Matrix Method for Wireless Communications*, 1st ed. (Cambridge University Press, Cambridge, 2014); C. Soize, *J. Sound Vib.* **263**, 893 (2003).
- [23] L. Zhao, S. Liao, Y. Wang, Z. Li, J. Tang, and B. Yuan, [arXiv:1703.00144v4](https://arxiv.org/abs/1703.00144v4) [cs.LG].
- [24] P. Shukla, *Phys. Rev. E* **62**, 2098 (2000); *J. Phys.: Condens. Matter* **17**, 1653 (2005).
- [25] A. D. Mirlin and F. Evers, *Rev. Mod. Phys.* **80**, 1355 (2008).
- [26] S. N. Evangelou and D. E. Katsanos, *J. Phys. A* **36**, 3237 (2003).
- [27] J. J. M. Verbaarschot, *Phys. Rev. Lett.* **72**, 2531 (1994).
- [28] R. M. Gray, *Found. Trends Commun. Info. Theory* **2**, 155 (2006).
- [29] T. Mondal, S. Sadhukhan, and P. Shukla, *Phys. Rev. E* **95**, 062102 (2017).
- [30] See Supplemental Material at <http://link.aps.org/supplemental/10.1103/PhysRevE.99.022124> for the derivation of Eqs. (3), (6), (7–11), and (27).
- [31] P. Shukla and S. Sadhukhan, *J. Phys. A* **48**, 415002 (2015).
- [32] S. Sadhukhan and P. Shukla, *Phys. Rev. E* **96**, 012109 (2017).
- [33] S. Sadhukhan and P. Shukla, *J. Phys. A* **48**, 415003 (2015).  $I_2(O_n) = 1$
- [34] O. Bohigas and M. J. Giannoni, *Ann. Phys.* **89**, 422 (1975).
- [35] J. M. G. Gomez, R. A. Molina, A. Relano, and J. Retamosa, *Phys. Rev. E* **66**, 036209 (2002).